

Contribution to the comparison of conventional concentric magnetic gear and double stage concentric magnetic gear for high power offshore wind applications

d'Almeida Renaud Philippe¹, Agbokpanzo Richard Gilles², Agbomahena Bienvenu Macaire¹

¹Department of Electrical Engineering, Polytechnic School of Abomey-Calavi (EPAC), Abomey-Calavi University (UAC), Cotonou, Benin

²Higher Normal School of Technical Education (ENSET), National University of Science, Technology, Engineering and Mathematics (UNSTM), Lokossa, Benin

Article Info

Article history:

Received Mar 25, 2023

Revised Jun 7, 2023

Accepted Jun 27, 2023

Keywords:

Concentric magnetic gear
Double-stage magnetic gear
Gear ratio
Indirect drive chain
Torque density

ABSTRACT

Nowadays, the replacement of mechanical technologies by magnetic technologies has several advantages. Therefore, in this paper, we compare in an indirect drive chain the conventional concentric magnetic gear (CCMG) and the double-stage concentric magnetic gear (DSCMG) used as a speed multiplier for a high-power offshore wind turbine. This comparison is performed for the same gear ratio and the same torque at the input of both magnetic gears to obtain the same torque values at the output of each gear. The goal is to determine which one has the smaller amount of magnet and the higher volumetric torque density. After the calculation of the gear ratio, a first choice of geometrical parameters is adopted. Several simulations carried out by the finite element method (FEM) allowed to obtain the desired torques and to fix the final geometrical parameters of each magnetic gear. The results obtained show that the DSCMG has both the smallest magnet volume and the highest volumetric torque density compared to the CCMG.

This is an open access article under the [CC BY-SA](https://creativecommons.org/licenses/by-sa/4.0/) license.



Corresponding Author:

d'Almeida Renaud Philippe

Department of Electrical Engineering, Polytechnic School of Abomey-Calavi (EPAC)

Abomey-Calavi University (UAC)

Cotonou, Littoral, Benin

Email: renaudjdd@yahoo.fr

NOMENCLATURE

G	: Gear ratio	ρ	: Air density
Ω_G	: Rated speed of the DFIG	C_p	: Turbine performance coefficient
Ω_{wt}	: Rated speed of the turbine	λ	: Tip speed ratio
f	: Frequency	s	: Slip in nominal operation
N_S	: Number of ferromagnetic pole pieces of the CCMG	B_r, B_θ	: Radial and tangential components of the magnetic flux density
p	: Number of pole pairs of the DFIG	c_f	: Cogging torque factor
P_{DFIG}	: Generator power	φ	: Scalar magnetic potential
R	: Radius of the turbine blade	R_i	: Radius of the inner rotor
T_{in}, T_{out}	: Input and output torque of the magnetic gear	μ_0	: Magnetic permeability of the vacuum
L_e	: Stack length of the magnetic gear	T_{DS}	: Volumetric torque density

B_{rin} ,	: Radial flux density of inner and	$B_{\theta in}$,	: Tangential flux density of inner and
B_{rout}	outer rotor	$B_{\theta out}$	outer rotor
V	: Total volume of the magnetic gear	P_f	: Iron losses
t_{rin} ,	: Inner and outer torque ripple coefficient	T_{av_in} ,	: Average input and output torque
t_{rout}		T_{av_out}	
T_{min_in}	: Minimum input torque	T_{max_out}	: Maximum output torque
T_{min_out}	: Minimum output torque	T_{max_in}	: Maximum input torque
N_{S1}, N_{S2}	: Number of ferromagnetic pole pieces of the first and second stage of the DSCMG	P_1, P_2	: Number of permanent magnet pole pairs of the inner and outer rotors of the CCMG
$P_{1,1}$,	: Number of permanent magnet pole pairs of the inner and outer rotors of the first stage	$P_{2,1}, P_{2,2}$: Number of permanent magnet pole pairs of the inner and outer rotors of the second stage
$P_{2,1}$			

1. INTRODUCTION

The demand for electrical energy is increasing day by day because of the growing population. To satisfy this demand, most countries harness their various renewable energy sources for clean power generation and boost their energy mix. Among the various renewable energy sources, wind energy occupies an important place in terms of installed generation capacity in the world. From the year 2011 to the year 2022, its generation capacity has increased from 238 GW to 845 GW [1]. Offshore wind power generation is very advantageous because the winds at sea are stronger and more regular. The development of offshore wind turbines offers promising prospects with the improvement of existing technologies [2]. For high power (above 1 MW) wind energy conversion systems (WECS) offshore it is essential to have systems that generate less loss and have good efficiency [3].

The WECS indirect drive chain consists of a turbine, a mechanical gear and a generator. Mechanical gears allow to transmit a high speed and a low torque to the generator shaft from a low speed and a high torque of the connected wind turbine. The mechanical gears used in offshore applications are often multi-stage planetary gears. Figure 1 shows this type of gearbox in the drive chain. Despite their important role, these mechanical gears are usually the weakest link in the wind power conversion system [4], [5]. This is because they are prone to several failures and their maintenance is very expensive [6]–[9]. The magnetic gears are the most promising alternative to the mechanical gears because of their high transmission and high torque density [10]. Compared to mechanical gears they operate without contact and generate low acoustic noise [11]. They offer several advantages, namely: improved reliability of WECS, reduced unplanned downtime, longer maintenance intervals, reduced labor costs and improved profitability of wind farms. All of these benefits contribute to the increased productivity and profitability of WECS.

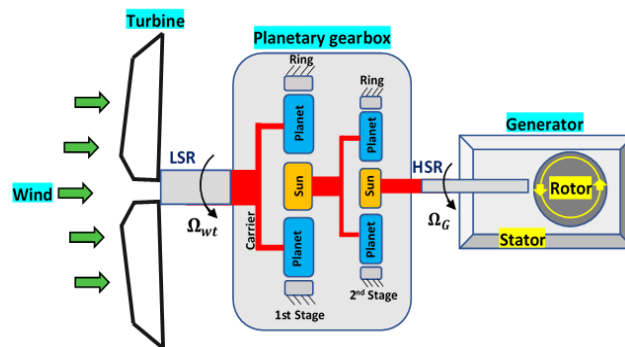


Figure 1. Indirect drive chain of WECS with mechanical gear

Several magnetic gear topologies have been proposed in the literature. However, it was in the early 2000s that the concentric magnetic gear proposed by [12] emerged as the most attractive topology. Figure 2 shows the concentric magnetic gear in the production chain. Therefore, several authors have extensively studied this type of magnetic gear in various fields of application [13]–[15]. Unfortunately, these studies have shown that magnetic gears also have their limitations. Due to the fact that they are based on permanent magnets, they induce eddy current losses which cause them to heat up [16]–[20]. On the other hand, in offshore applications, the torques to be developed are very large and lead to bulky magnetic gears with large quantities of magnets. However, the cost of permanent magnets, especially in rare earth, is very high. These

different aspects limit their design and their use in high power WECS. It is in this context that in this paper we compare the CCMG and the DSCMG when they are each connected at their output to the shaft of a 1.633 MW double fed induction generator (DFIG). The objective here is to see between the two magnetic gears the one that will be much more reliable and economically profitable.

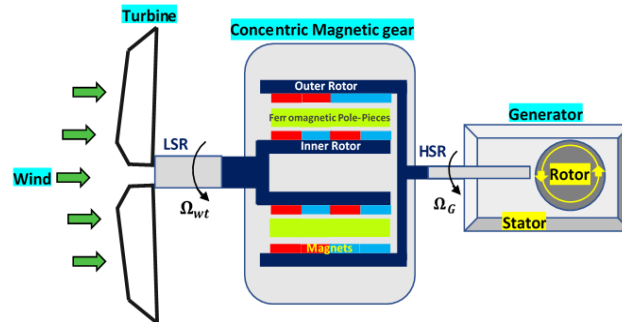


Figure 2. Indirect drive chain of WECS with concentric magnetic gear

This paper is divided into three parts. In the first part the description and the principle of operation of each of the two magnetic gears is presented. The second part deals with the sizing methodology of each of the magnetic gears and finally the third part is devoted to the analysis of the obtained results.

2. DESCRIPTION AND OPERATION OF THE STUDIED MAGNETIC GEARS

The topologies of the two studied magnetic gears are shown in Figure 3. In the drive chain, the configuration adopted for each of the two magnetic gears is to connect the low speed rotor of the turbine to the inner rotor shaft of the magnetic gear and the high-speed rotor of the DFIG to the outer rotor shaft of the magnetic gear. The CCMG gear shown in Figure 3(a) consists of two rotors, one of which is inside and the other outside. Between the two rotors are the ferromagnetic pole pieces. Each rotor contains permanent magnets on its inner (for the outer rotor) and outer (for the inner rotor) surface. It can be noticed that there are more permanent magnet pole pairs on the inner rotor than on the outer rotor. The inner rotor is therefore the low speed rotor. When the wind turbine is connected to the inner rotor, it rotates at low speed and the permanent magnets of the inner rotor create a magnetic field through the ferromagnetic pole pieces. The modulation of this magnetic field by the ferromagnetic pole pieces interacts with the magnetic field created by the permanent magnets of the outer rotor and forces it to rotate at high speed in the opposite direction [21], [22]. This allows the shaft of the DFIG connected to the external rotor to rotate at high speed.

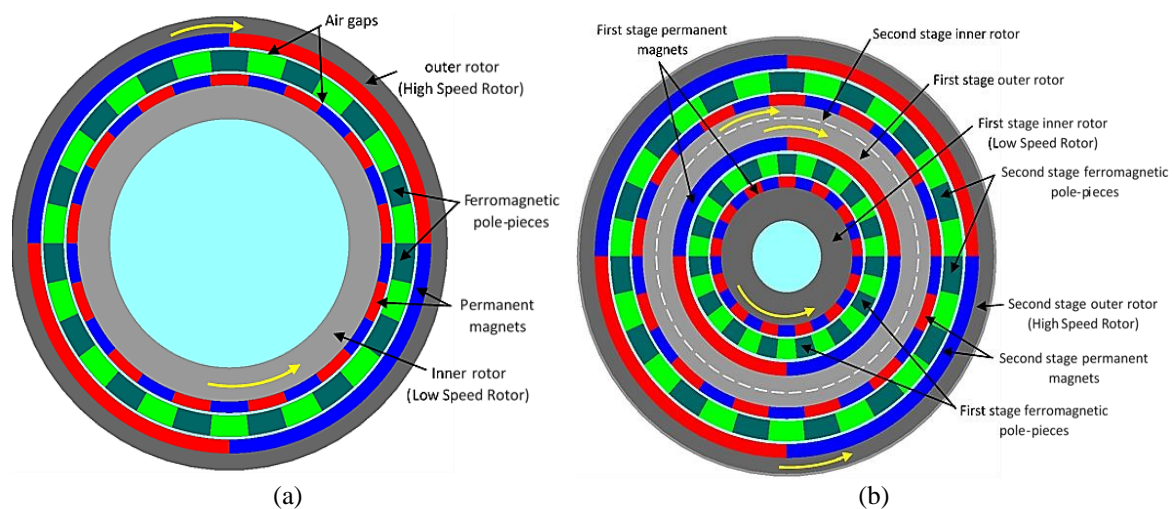


Figure 3. Topology of (a) CCMG and (b) DSCMG

The DSCMG is shown in Figure 3(b). The first stage is distinguished from the second stage by the concentric circle shown in white in the figure. It consists of two concentric magnetic gears, one of which is inside the other. The first magnetic gear is the first stage and the second is the second stage. They both share a common rotor. It can be seen that in the first stage, the inner rotor has the greatest number of permanent magnet poles. It represents the low-speed rotor connected to the wind turbine. At the second stage, the outer rotor has the least number of permanent magnet poles. It represents the high-speed rotor connected to the shaft of the DFIG. The operation of this magnetic velocity multiplier is similar to the conventional magnetic multiplier with the only difference that the torque transmission is done between two stages: from the first stage to the second stage.

3. METHODOLOGY FOR COMPARING THE CCMG AND DSCMG

To compare the two magnetic gears, it is necessary to size them for the same gear ratio G . The flowchart proposed in Figure 4 indicates the steps to be followed for the sizing. The gear ratio G is calculated by (1), where Ω_G and Ω_{wt} are the respective nominal velocities of the DFIG and the turbine. They are defined by (2) and (3) [23], [24].

$$G = \frac{\Omega_G}{\Omega_{wt}} \quad (1)$$

$$\Omega_G = \frac{2\pi f(1-s)}{p} \quad (2)$$

Where f is the frequency in Hz; s is the slip in nominal operation; and p is the number of pole pairs of the DFIG.

$$\Omega_{wt} = \frac{\lambda}{R} \left(\frac{2P_{DFIG}}{C_p \rho \pi R^2} \right)^{\frac{1}{3}} \quad (3)$$

Where P_{DFIG} is the generator power (MW); R is the radius of the turbine blade (m); ρ is the air density (kg/m^3); C_p is the turbine performance coefficient; and λ is the tip speed ratio. The DFIG parameters used are listed in Table 1.

Table 1. The DFIG parameters

Parameters (unit)	Value	Parameters (unit)	Value
P_{DFIG} (MW)	1.633	λ	6.908
C_p	0.44	f (Hz)	50
ρ (kg/m^3)	1.225	s	0.02
R (m)	35	p	2

The gear ratio G expressed by (1) is again a function of the numbers of pole pairs of permanent magnets at each magnetic gear. This ratio is described by (4) for the CCMG and (5) for the DSCMG [25].

$$G = \frac{P_1}{P_2} \quad (4)$$

Where P_1 and P_2 are respectively the number of permanent magnet pole pairs of the inner and outer rotors of the CCMG.

$$G = G_1 \times G_2 \quad (5)$$

With G_1 and G_2 the respective gear ratio of the first and second stage defined by the following system:

$$\begin{cases} G_1 = \frac{P_{1,1}}{P_{2,1}} \\ G_2 = \frac{P_{1,2}}{P_{2,2}} \end{cases} \quad (6)$$

Where $P_{1,1}$ and $P_{2,1}$ are respectively the number of pole pairs of permanent magnets of the inner and outer rotors of the first stage of the DSCMG. Similarly, $P_{2,1}$ and $P_{2,2}$ are respectively the number of pole pairs of permanent magnets of the inner and outer rotors of the second stage of the DSCMG.

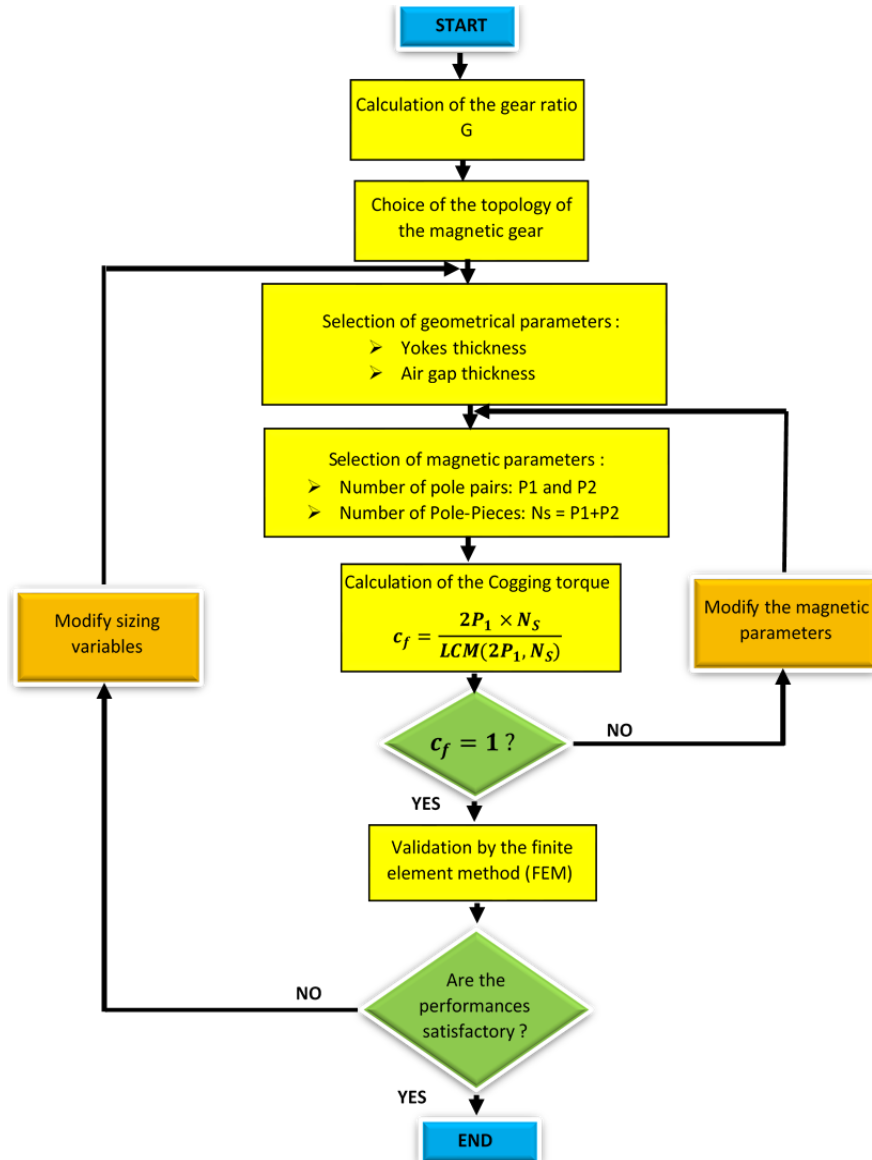


Figure 4. Sizing flowchart of the studied magnetic gears

The numbers of ferromagnetic pole pieces N_s for the CCMG and N_{s1} and N_{s2} respectively for the first and second stage of the DSCMG must satisfy the following relationships:

$$\begin{cases} N_s = P_1 + P_2 \\ N_{s1} = P_{1,1} + P_{2,1} \\ N_{s2} = P_{1,2} + P_{2,2} \end{cases} \quad (7)$$

The cogging torque factor (c_f) whose expression is presented in (8) must be close to the value 1 to reduce torque ripples as much as possible. This coefficient is calculated in the same way at the DSCMG level by replacing N_s and P_1 by N_{s1} and $P_{1,1}$ at the first stage and N_s and P_1 by N_{s2} and $P_{1,2}$ at the second stage [26].

$$c_f = \frac{2P_1 \times N_s}{LCM(2P_1, N_s)} \quad (8)$$

We impose subsequently that c_f is to be equal to 1 in order to have the best combinations (P_1, N_s) , $(P_{1,1}, N_{s1})$, and $(P_{1,2}, N_{s2})$.

The magnetic parameters $P_1, P_2, P_{1,1}, P_{1,2}, P_{2,1}, P_{2,2}, N_s, N_{s1},$ and N_{s2} are therefore selected by strictly adhering to (1) through (8) listed above. The radial B_r and tangential B_θ components of the magnetic flux density are described by (9) and (10) [27].

$$B_r = -\mu_0 \frac{\partial \varphi}{\partial r} \quad (9)$$

$$B_\theta = -\frac{\mu_0}{r} \frac{\partial \varphi}{\partial \theta} \quad (10)$$

Where φ represent the scalar magnetic potential and μ_0 is the magnetic permeability of the vacuum.

The input torque T_{in} and output torque T_{out} of each magnetic gear are given by (11).

$$\begin{cases} T_{in} = \frac{P_{DFIG}}{\Omega_{wt}} \\ T_{out} = \frac{T_{in}}{G} \end{cases} \quad (11)$$

The relationship (11) allows the analytical calculation of the desired input and output torques of each magnetic gear. The torque T_{in} developed by inner rotor of each gear is also defined as (12) [28].

$$T_{in} = \frac{L_e R_i^2}{\mu_0} \int_0^{2\pi} (B_{rin} + B_{rout})(B_{\theta in} + B_{\theta out}) d\theta \quad (12)$$

Where R_i is the radius of the inner rotor; L_e is the Stack length of the magnetic gear; B_{rin}, B_{rout} and $B_{\theta in}, B_{\theta out}$ are respectively the radial and tangential flux density of inner and outer rotor. With $\int_0^{2\pi} B_{rin} B_{\theta in} d\theta = 0$ and $\int_0^{2\pi} B_{rout} B_{\theta out} d\theta = 0$ the simplified analytical expression of (12) is (13).

$$T_{in} = \pi \mu_0 L_e R_i^2 \sum_{n=1}^{\infty} [(P_{n,out} S_{n,in} + Q_{n,out} R_{n,in}) + (P_{n,in} S_{n,out} + Q_{n,in} R_{n,out})] \quad (13)$$

Where:

$$P_{n,in} = n(E_{n,in} R_i^{n-1} - F_{n,in} R_i^{-n-1}) \quad (14)$$

$$Q_{n,in} = n(G_{n,in} R_i^{n-1} - H_{n,in} R_i^{-n-1}) \quad (15)$$

$$R_{n,in} = -n(E_{n,in} R_i^{n-1} + F_{n,in} R_i^{-n-1}) \quad (16)$$

$$S_{n,in} = n(G_{n,in} R_i^{n-1} + H_{n,in} R_i^{-n-1}) \quad (17)$$

$$P_{n,out} = n(E_{n,out} R_i^{n-1} - F_{n,out} R_i^{-n-1}) \quad (18)$$

$$Q_{n,out} = n(G_{n,out} R_i^{n-1} - H_{n,out} R_i^{-n-1}) \quad (19)$$

$$R_{n,out} = -n(E_{n,out} R_i^{n-1} + F_{n,out} R_i^{-n-1}) \quad (20)$$

$$S_{n,out} = n(G_{n,out} R_i^{n-1} + H_{n,out} R_i^{-n-1}) \quad (21)$$

with $E_{n,in}, E_{n,out}, F_{n,in}, F_{n,out}, G_{n,in}, G_{n,out}, H_{n,in},$ and $H_{n,out}$ constants.

After the calculation of the gear ratio, and the selection of the magnetic parameters, a first standard choice of the geometrical parameters (thickness of the yokes, thickness of the permanent magnets, thickness of the ferromagnetic pole pieces, internal and external radii of the rotors) of each magnetic gear is established. Several simulations are then performed in dynamic operation by the FEM. The Flux-2D version 2022 finite element analysis software is used here. When the desired torques (T_{in} and T_{out}) are reached, the simulation is stopped and the geometrical parameters obtained are fixed. These parameters are final for each magnetic gear. We deduce the elements we need for the comparison. This comparison is done at various levels, namely: the comparison of permanent magnets volumes, volumetric torque densities, eddy current losses in the magnets, iron losses in the rotor yokes and torques ripple.

The calculation of the volumetric torque density (T_{DS}) is done analytically using the (22) [15].

$$T_{DS} = \frac{T_{in}}{V} \quad (22)$$

Where V is the total volume of the magnetic gear. For the calculation of the iron losses (P_f) the Flux2D software uses (23) based on the Bertotti method [29].

$$P_f = k_1 f B^{\alpha_1} + k_2 (f \cdot B)^{\alpha_2} + k_3 (f \cdot B)^{\alpha_3} \quad (23)$$

With B : flux density, $k_1 f B^{\alpha_1}$: hysteresis losses, $k_2 (f \cdot B)^{\alpha_2}$: eddy current losses, and $k_3 (f \cdot B)^{\alpha_3}$: losses by excess. The eddy current losses in the magnets are also obtained after simulation.

In order to compare the stability of the inner and outer torques of each magnetic gear, the torque ripple coefficient is calculated after simulation. The inner torque ripple t_{rin} is given by (24) [30].

$$t_{rin} = \frac{T_{\max_in} - T_{\min_in}}{T_{av_in}} \quad (24)$$

Where T_{\max_in} is the maximum input torque value; T_{\min_in} is the minimum input torque value; and T_{av_in} is the average input torque value. The same in (24) is used to calculate outer torque ripple by substituting inner torques with outer torques values.

4. RESULTS AND DISCUSSION

The gear ratio calculated from (1) give $G = 54.7$. The speed of the generator in nominal operation is 1,800 rpm and that of the wind turbine is 32.9 rpm. Thus, these speeds are respectively imposed on the generator shaft and the turbine shaft. After the various simulations made with the FEM, the geometrical parameters obtained for each gear are shown in Table 2.

Table 2. Geometrical parameters of each magnetic gear

Parameters (unit)	CCMG	DSCMG	
	Value	First stage value	Second stage value
Number of pole pairs of the inner rotor	164	53	58
Number of pole pairs of the outer rotor	3	8	7
Number of ferromagnetic Pole-Pieces	167	61	65
Thickness of the inner air gap (mm)	2	2	2
Thickness of the outer air gap (mm)	2	2	2
Thickness of the ferromagnetic Pole-Pieces (mm)	30	30	5.78
Thickness of the permanent magnets of the inner rotor (mm)	25	25	5
Thickness of the permanent magnets of the outer rotor (mm)	25	25	5
Thickness of the inner rotor yoke (mm)	45	45	16.5
Thickness of the outer rotor yoke (mm)	45	45	10.76
Internal radius of the magnetic gear (mm)	850	451.5	625.5
External radius of the magnetic gear (mm)	1,024	625.5	672.54
Stack length (m)	2	2	2

At the level of the CCMG, the flux density map is shown in Figure 5. The curves of the inner and outer torques are presented in Figure 6. Similarly, the flux density variations in the inner and outer air gaps are shown in Figures 7 and 8 respectively.

It is clear from Figure 5 that the maximum flux density reached is 3.008T. As described in the methodology, the turbine shaft is connected to the inner rotor and the generator shaft to the outer rotor. In this configuration, the inner rotor must rotate at low speed, developing a high inner torque. The outer rotor must rotate at high speed in the opposite direction, developing a low outer torque relative to the inner rotor. The gear ratio is kept constant during speed and torque transmissions between the two rotors.

Figure 6 shows that the average torque at the input of the inner rotor is 3.8×10^5 Nm. This is considerably higher than the torque transmitted at the output of the outer rotor, which is 6.97×10^3 Nm. The two torques plotted on this figure are opposite in sign. This explains why the two rotors rotate in opposite directions. This result is logical given the configuration we've adopted, which enables us to use the CCMG as a speed multiplier on the outer rotor.

In Figures 7 and 8, the maximum flux density reached in the middle of the inner and outer air gaps are 1.131T and 1.089T respectively. It can be seen that the magnetic field amplitude in the middle of the inner air gap is greater than that of the outer air gap. This is because there are significantly more permanent magnet pole pairs in the inner rotor than the outer.

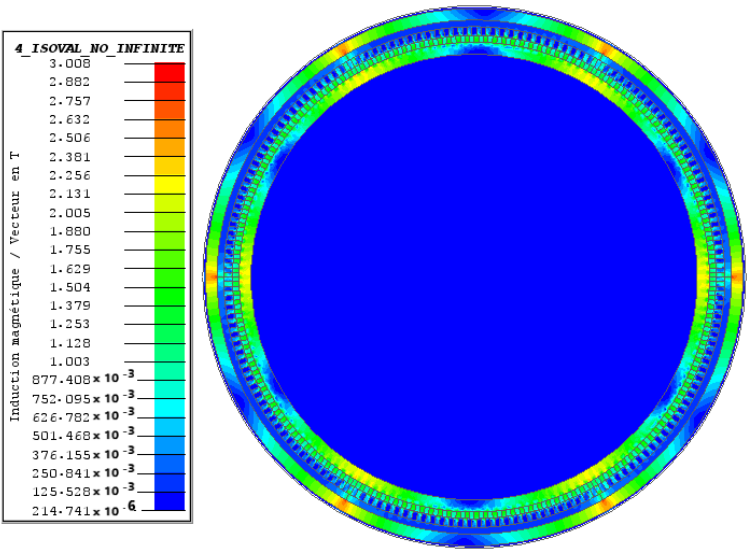


Figure 5. Magnetic flux density map in the CCMG

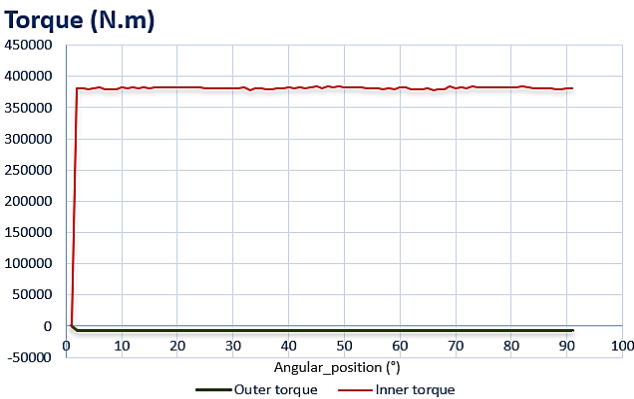


Figure 6. Torques curves in the CCMG

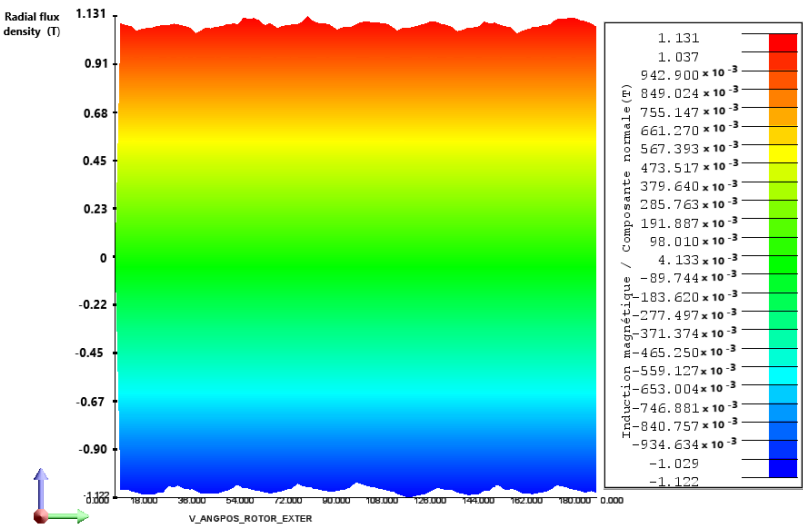


Figure 7. Flux density variations in the inner air gap

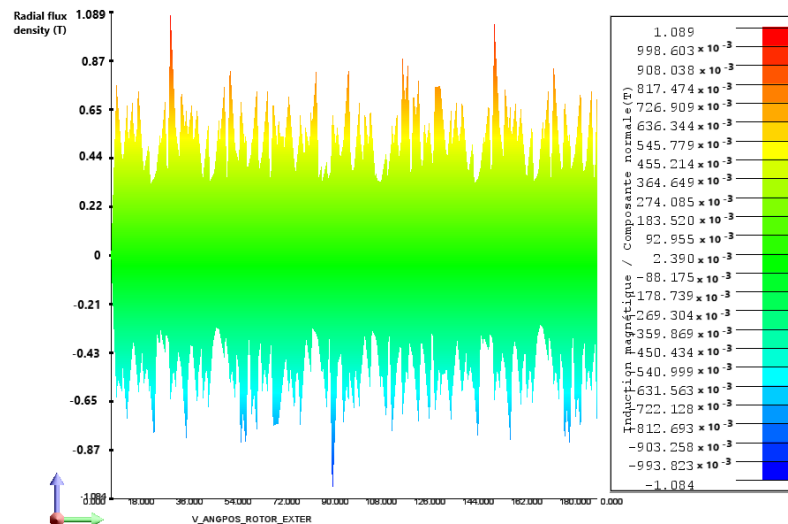


Figure 8. Flux density variations in the outer air gap

The volumes of the magnets used in the inner and outer rotors are 0.2851 m^3 and 0.3036 m^3 respectively. The total volume of the CCMG is 2.0488 m^3 . Each stage of the DSCMG is simulated separately while respecting the constraints related to the common rotor. That is, the speeds and torques of the outer rotor of the first stage and the inner rotor of the second stage must be the same. The results of the first stage are presented in Figures 9 to 12.

In the first stage of the DSCMG, the maximum flux density given by the flux density map in Figure 9 is 3.655T. The inner rotor of the first stage is connected to the turbine shaft. Consequently, its torque amplitude must be greater than its outer rotor amplitude. Figure 10 shows that the input torque developed at the first-stage inner rotor is $3.8 \times 10^5 \text{ Nm}$. This torque is the same as that applied at the CCMG input. At the output of the first stage, the average torque is $5.74 \times 10^4 \text{ Nm}$ lower than the inner torque. This is quite normal, since the first stage is also used as a speed multiplier at its output. What's more, the curves for the two torques have opposite signs. This proves that the two rotors of the first stage rotate in opposite directions.

Figures 11 and 12 show, respectively, the variations of radial flux density in the middle of the air gaps of the inner and outer rotors of the first stage. The maximum flux density value for the inner rotor is 2.01T, higher than that for the outer rotor, which is 1.672T. This result can be seen from the higher number of permanent magnet pole pairs in the inner rotor as compared with the outer rotor. The magnet volumes used in the first stage are 0.16 m^3 for the inner rotor and 0.178 m^3 for the outer rotor.

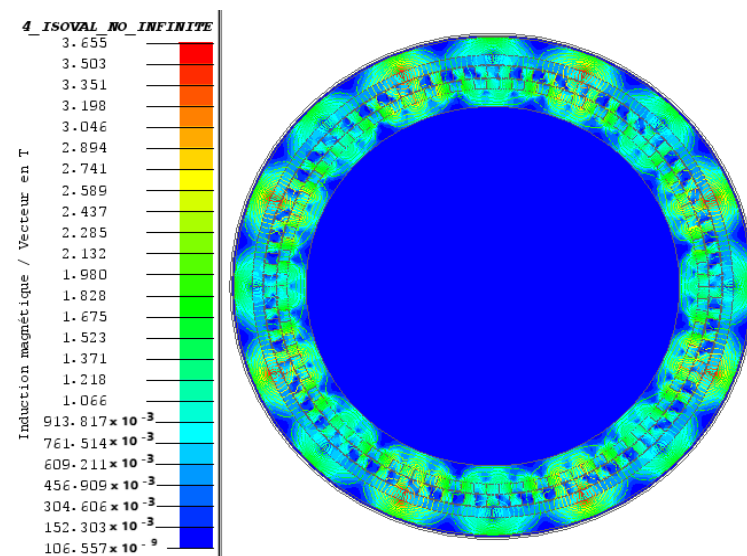


Figure 9. Flux density map in the first stage

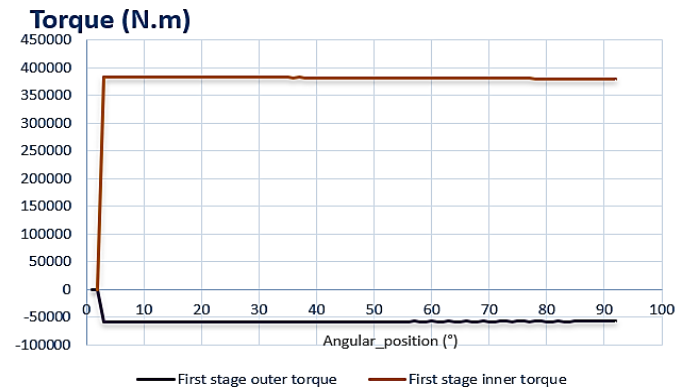


Figure 10. Torques curves in the first stage

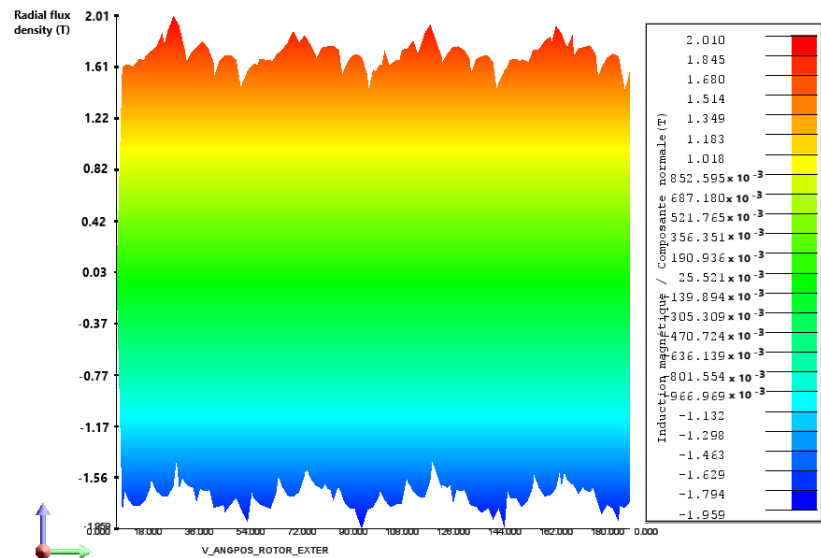


Figure 11. Flux density variations in the inner air gap

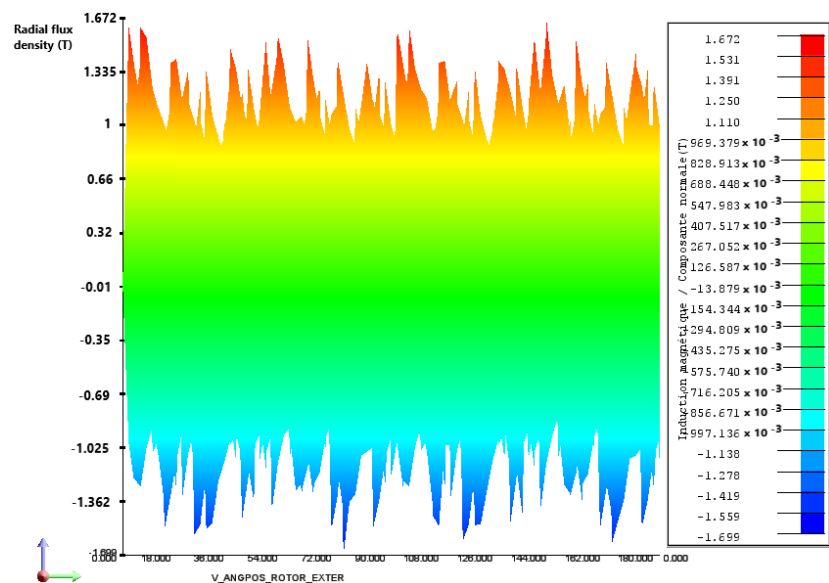


Figure 12. Flux density variations in the outer air gap

Second-stage results from the DSCMG are presented in Figures 13 to 16. Figure 13 shows the flux density map of the second stage. The maximum flux density given by this map is 2.819T. The inner and outer torques of the second stage are plotted in Figure 14. It can be seen that the average input torque of the second stage is 5.74×10^4 Nm. This torque is equal to the average torque at the output of the first stage, since the first and second stages share a common rotor. The second-stage output is connected to the high-speed generator shaft. The output torque of the second stage should consequently be lower than the input torque. This is the case in this application, since the second-stage output torque is 6.94×10^3 Nm. The inner and outer rotors of the second stage rotate in opposite directions because their torques have opposite signs. The output torque of the second stage is approximately equal to the output torque of the CCMG, as expected for the comparison of the two magnetic gears.

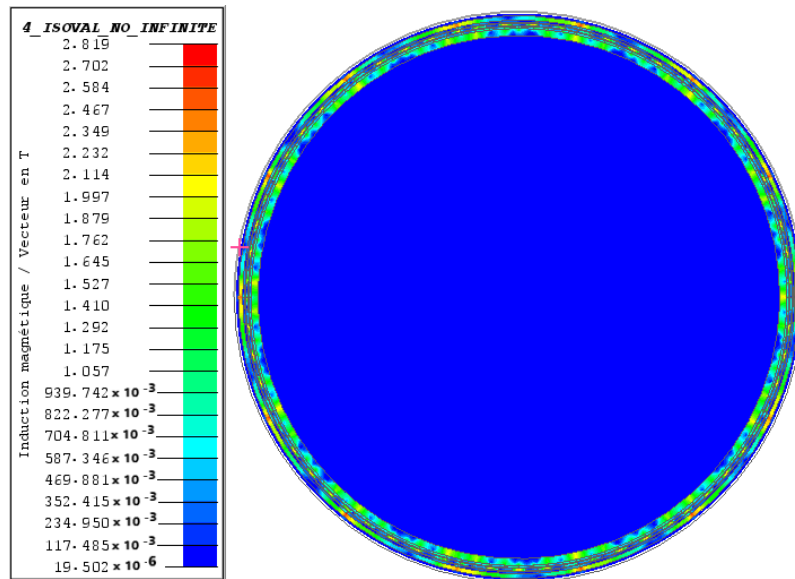


Figure 13. Flux density map in the second stage

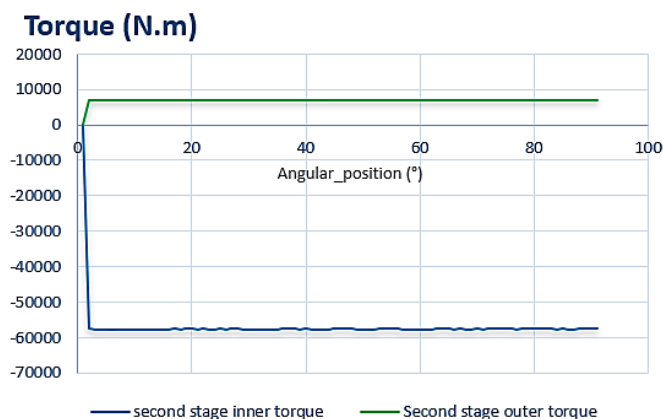


Figure 14. Torques curves in the second stage

Figures 15 and 16 show the radial flux density variations at the center of the inner and outer air gaps of the second stage. The maximum flux density in the inner and outer air gap of the second stage are respectively 1.326 T and 1.106 T. The amplitude of the flux density of the inner rotor is greater than the outer rotor because there are more permanent magnet pole pairs in the inner rotor than the outer rotor. The magnet volumes obtained in the second stage are 0.0405 m^3 in the inner rotor and 0.0414 m^3 in the outer rotor. The total volume of the DSCMG is 1.5611 m^3 .

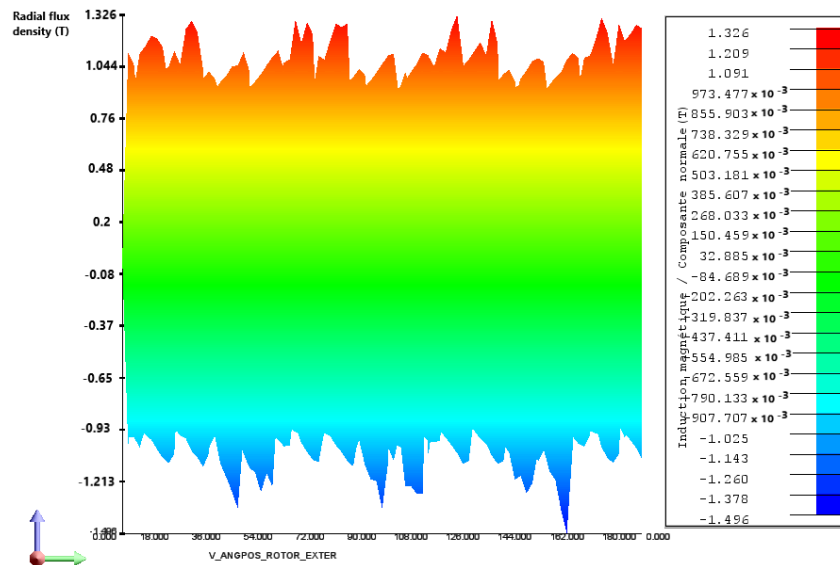


Figure 15. Flux density variations in the inner air gap

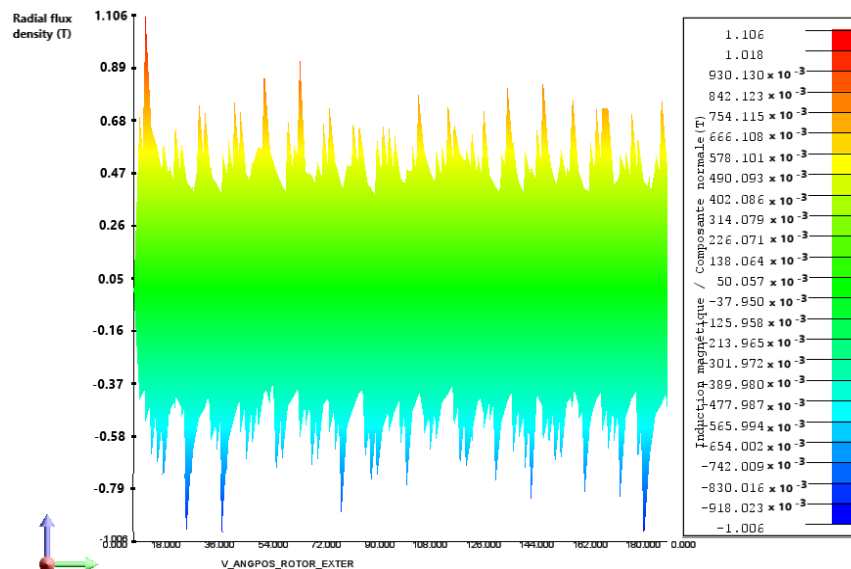


Figure 16. Flux density variations in the outer air gap

Table 3 shows the comparative values of the results obtained. It can be seen that the total volume of permanent magnets used at CCMG is 0.5887 m^3 . This volume is significantly higher than the total volume used in the DSCMG which is 0.42 m^3 . This result shows that there will be less eddy current losses in the DSCMG magnets than in the CCMG magnets. This is justified by the eddy current losses found after simulation which give values of 94.24 kW at the CCMG and only 23 kW at the DSCMG. These values prove that there are about four times more eddy current losses in the CCMG magnets than in the DSCMG magnets.

The volumetric torque density of the DSCMG is 243.42 kNm/m^3 . This density is significantly better than that of the CCMG which is only 185.47 kNm/m^3 . Moreover, the iron losses of the CCMG are 84.8 kW . These losses are more than twice as high as those of the DSCMG which are 41.36 kW .

Table 4 shows the torque ripples calculated at the inner and outer rotors of each magnetic gear. It can be seen that the inner and outer torque ripples of the CCMG are 1.55% and 15.51% respectively. There is therefore more stability of torque at the output of the inner rotor than at the outer rotor of the CCMG. Similarly, on the DSCMG, the torque ripples of the inner and outer rotors are 0.97% and 4.12% respectively. We also note that there is more stability of torque at the output of the DSCMG's inner rotor than at its outer rotor.

Table 3. Comparative values of CCMG and DSCMG

	Conventional concentric magnetic gear (CCMG)	Double-stage concentric magnetic gear (DSCMG)	
		First stage	Second stage
Generator power (MW)	1.633	1.633	
Gear ratio	54.7	6.6	8.29
Total gear ratio	54.7	54.7	
Input torque (N.m)	3.8×10^5	3.8×10^5	5.74×10^4
Output torque (N.m)	6.97×10^3	5.74×10^4	6.94×10^3
Internal magnets volume (m ³)	0.2851	0.16	0.0405
External magnets volume (m ³)	0.3036	0.178	0.0414
Total volume of magnets (m ³)	0.5887		0.42
Volume of magnetic gear (m ³)	2.0488		1.5611
Volumetric torque density (kNm/m ³)	185.47		243.42
		14.79	8.212
Eddy current losses (kW)	94.24	23	
		3.19	38.17
Iron losses (kW)	84.8		41.36

Table 4. Torques ripple comparison

	Conventional concentric magnetic gear (CCMG)	Double-stage concentric magnetic gear (DSCMG)
Maximum input torque T_{\max_in} (N.m)	3.841×10^5	3.829×10^5
Minimum input torque T_{\min_in} (N.m)	3.782×10^5	3.792×10^5
Average input torque T_{av_in} (N.m)	3.8×10^5	3.8×10^5
Inner torque ripple t_{rin} (%)	1.55	0.97
Maximum output torque T_{\max_out} (N.m)	7.587×10^3	7.085×10^3
Minimum output torque T_{\min_out} (N.m)	6.506×10^3	6.799×10^3
Average output torque T_{av_out} (N.m)	6.97×10^3	6.94×10^3
Outer torque ripple t_{rout} (%)	15.51	4.12

When we compare the torque ripples of the CCMG and the DSCMG, we notice that the torque ripple at the inner rotor of the DSCMG is lower than that of the CCMG. This torque ripple is reduced by 37.42% at the inner rotor of the DSCMG compared with that of the CCMG. It can be affirmed that the inner rotor of the DSCMG is more stable than that of the CCMG. Similarly, the torque ripple of the DSCMG outer rotor is significantly lower than that of the CCMG outer rotor. The torque ripple of the outer rotor of the DSCMG is reduced this time by 73.44% compared with that of the CCMG. Output torque stability of the DSCMG outer rotor is therefore significantly improved compared with that of the CCMG. We can deduct from these results that the DSCMG is more stable than the CCMG in torque transmission. It presents less torque ripple at the inner and outer rotor than the CCMG.

From these various comparisons, it can be concluded that in the same high-power offshore power train, the choice of DSCMG is more advantageous than that of CCMG. This is because the DSCMG is less cumbersome because of its small volume compared to the CCMG. In addition, the DSCMG has less losses and its torque density is higher than that of the CCMG. The DSCMG also transmits a more stable torque with less ripple than the CCMG.

5. CONCLUSION

The improvement of wind energy technologies requires high performance drive systems with good reliability, low cost and high efficiency. The replacement of mechanical gears by magnetic gears in WECS represents one of the best solutions to obtain good performances. However, magnetic technologies generate enough heat which usually degrades their efficiency especially when used to develop high torque and power. In WECS used offshore it is important to see which type or topology of magnetic gears will be more suitable and economically viable. This work shows the comparison between two magnetic gears able to be used in a high-power indirect wind energy production chain. Each of the two magnetic gears, namely the CCMG and the DSCMG, are sized and used here as speed multipliers on the external rotor to drive the DFIG shaft. For the same gear ratio of 54.7 and the same average torque of 3.8×10^5 N.m applied at the input of each magnetic gear's inner rotors, the FEM simulation gives approximately the same torque values at the output of each magnetic gear. The torque density of the DSCMG is 23.81% better than that of the CCMG. The DSCMG has around four times less eddy current losses and two times fewer iron losses than the CCMG. Torque ripple analysis showed that the DSCMG's inner-rotor torque ripple is reduced by 37.42%, and its outer-rotor torque ripple is also reduced by 73.44% compared to the CCMG. The DSCMG therefore has the smallest magnet

volume, the highest torque density, the best torque transmission stability and the best efficiency compared to the CCMG. Therefore, DSCMG will be more cost effective to use in WECS than CCMG. Further studies on loss reduction of DSCMG will be required to improve its performance for its design.

Despite their ability to validly replace mechanical gears, the two magnetic gears compared are quite bulky and their design remains complex. The design of the DSCMG remains more complex than that of the CCMG. This is because it has three rotors and two modulating rings. In addition, a large quantity of magnet is used in each magnetic gear. This can significantly increase the cost of their design, due to the high cost of rare-earth permanent magnets.




REFERENCES

- [1] D. Henner and REN21, "Renewables 2022 global status report 2022," p. 309, 2022.
- [2] L. Jian, G. Xu, Y. Gong, J. Song, J. Liang, and M. Chang, "Electromagnetic design and analysis of a novel magnetic-gear-integrated wind power generator using time-stepping finite element method," *Progress in Electromagnetics Research*, vol. 113, pp. 351–367, 2011, doi: 10.2528/PIER10121603.
- [3] A. Bensalah, G. Barakat, and Y. Amara, "Electrical Generators for Large Wind Turbine: Trends and Challenges," *Energies*, vol. 15, no. 18, 2022, doi: 10.3390/en15186700.
- [4] W. Musial, S. Butterfield, and B. McNiff, "Improving wind turbine gearbox reliability," *European Wind Energy Conference and Exhibition 2007, EWEC 2007*, vol. 3, pp. 1770–1779, 2007.
- [5] D. S. Painter, "A Comparative Study of the Performance Capabilities of Magnetic Gears," 2016.
- [6] A. Leontaritis, A. Nassehi, and J. M. Yon, "A Monte Carlo Analysis of the Effects of Geometric Deviations on the Performance of Magnetic Gears," *IEEE Transactions on Industry Applications*, vol. 56, no. 5, pp. 4857–4869, 2020, doi: 10.1109/TIA.2020.3008115.
- [7] W. Teng, X. Ding, X. Zhang, Y. Liu, and Z. Ma, "Multi-fault detection and failure analysis of wind turbine gearbox using complex wavelet transform," *Renewable Energy*, vol. 93, pp. 591–598, 2016, doi: 10.1016/j.renene.2016.03.025.
- [8] K. Atallah, S. D. Calverley, and D. Howe, "Design, analysis and realisation of a high-performance magnetic gear," *IEE Proceedings: Electric Power Applications*, vol. 151, no. 2, pp. 135–143, 2004, doi: 10.1049/ip-epa:20040224.
- [9] D. Fodorean, "State of the Art of Magnetic Gears, their Design, and Characteristics with Respect to EV Application," *Modeling and Simulation for Electric Vehicle Applications*, 2016, doi: 10.5772/64174.
- [10] M. Desvaux, B. Multon, H. Ben Ahmed, and S. Sire, "Behaviour comparison between mechanical epicyclic gears and magnetic gears," *Mechanisms and Machine Science*, vol. 54, pp. 401–410, 2018, doi: 10.1007/978-3-319-67567-1_38.
- [11] P. O. Rasmussen, T. O. Andersen, F. T. Jørgensen, and O. Nielsen, "Development of a high-performance magnetic gear," *IEEE Transactions on Industry Applications*, vol. 41, no. 3, pp. 764–770, 2005, doi: 10.1109/TIA.2005.847319.
- [12] K. Atallah and D. Howe, "A novel high-performance magnetic gear," *IEEE Transactions on Magnetics*, vol. 37, no. 4 I, pp. 2844–2846, 2001, doi: 10.1109/20.951324.
- [13] K. B. and N. Khenfer, "Magnetic gear generator for wind energy," *PRZEGLĄD ELEKTROTECHNICZNY*, vol. 89, no. 5, pp. 72–75, 2013.
- [14] M. Cheng, L. Sun, G. Buja, and L. Song, "Advanced electrical machines and machine-based systems for electric and hybrid vehicles," *Energies*, vol. 8, no. 9, pp. 9541–9564, 2015, doi: 10.3390/en8099541.
- [15] H. Baninajar, S. Modaresahmadi, H. Y. Wong, J. Z. Bird, W. Williams, and B. Dechant, "Experimental Evaluation of a 63.3:1 Dual-Stage Coaxial Magnetic Gear," *IEEE Transactions on Energy Conversion*, vol. 38, no. 1, pp. 158–169, 2023, doi: 10.1109/TEC.2022.3190831.
- [16] V. Mateev, I. Marinova, and M. Todorova, "Eddy current losses in permanent magnets of a coaxial magnetic gear," *2018 20th International Symposium on Electrical Apparatus and Technologies, SIELA 2018 - Proceedings*, 2018, doi: 10.1109/SIELA.2018.8447082.
- [17] M. Desvaux, S. Sire, S. Hlioui, H. Ben Ahmed, and B. Multon, "Development of a hybrid analytical model for a fast computation of magnetic losses and optimization of coaxial magnetic gears," *IEEE Transactions on Energy Conversion*, vol. 34, no. 1, pp. 25–35, 2019, doi: 10.1109/TEC.2018.2858859.
- [18] Y. Zhang, K. Lu, and Y. Ye, "Permanent magnet eddy current loss analysis of a novel motor integrated permanent magnet gear," *IEEE Transactions on Magnetics*, vol. 48, no. 11, pp. 3005–3008, 2012, doi: 10.1109/TMAG.2012.2200663.
- [19] M. Filippini *et al.*, "Magnetic loss analysis in coaxial magnetic gears," *Electronics (Switzerland)*, vol. 8, no. 11, 2019, doi: 10.3390/electronics8111320.
- [20] Y. C. Wu, F. M. Ou, M. C. Tsai, and S. N. Fajri, "Development of a Dual-Input Magnetic Gear Train for the Transmission System of Small-Scale Wind Turbines," *Applied Sciences (Switzerland)*, vol. 12, no. 7, 2022, doi: 10.3390/app12073685.
- [21] M. Johnson, S. Englebreton, M. C. Gardner, W. Ouyang, H. A. Toliyat, and C. Tschida, "Design, construction, and analysis of a large scale inner stator radial flux magnetically geared generator for wave energy conversion," *2017 IEEE Energy Conversion Congress and Exposition, ECCE 2017*, vol. 2017-Janua, pp. 5017–5024, 2017, doi: 10.1109/ECCE.2017.8096848.
- [22] M. C. Gardner, M. Johnson, and H. A. Toliyat, "Analysis of High Gear Ratio Capabilities for Single-Stage, Series Multistage, and Compound Differential Coaxial Magnetic Gears," *IEEE Transactions on Energy Conversion*, vol. 34, no. 2, pp. 665–672, 2019, doi: 10.1109/TEC.2018.2868730.
- [23] H. Li and Z. Chen, "Design optimization and evaluation of different wind generator systems," *Proceedings of the 11th International Conference on Electrical Machines and Systems, ICEMS 2008*, pp. 2396–2401, 2008.
- [24] R. Gianto, "Constant Power Factor Model of DFIG-Based Wind Turbine for Steady State Load Flow Studies," *Energies*, vol. 15, no. 16, 2022, doi: 10.3390/en15166077.
- [25] A. Floris, A. Serpi, M. Porru, G. Fois, and A. Damiano, "Design of a double-stage magnetic gear for high-speed electric propulsion systems," *Proceedings - 2018 23rd International Conference on Electrical Machines, IECM 2018*, pp. 670–676, 2018, doi: 10.1109/ICELMACH.2018.8506911.
- [26] Z. Q. Zhu and D. Howe, "Influence of design parameters on cogging torque in permanent magnet machines," *IEEE Transactions on Energy Conversion*, vol. 15, no. 4, pp. 407–412, 2000, doi: 10.1109/60.900501.
- [27] L. Jian and K. T. Chau, "Analytical calculation of magnetic field distribution in coaxial magnetic gears," *Progress in Electromagnetics Research*, vol. 92, pp. 1–16, 2009, doi: 10.2528/PIER09032301.




- [28] P. Tzouganakis, V. Gakos, C. Kalligeros, A. Tsolakis, and V. Spitas, "Fast and efficient simulation of the dynamical response of coaxial magnetic gears through direct analytical torque modelling," *Simulation Modelling Practice and Theory*, vol. 123, 2023, doi: 10.1016/j.simpat.2022.102699.
- [29] "Modified Bertotti model identification tool." Accessed: Oct. 13, 2023. [Online]. Available: <https://2021.help.altair.com/2021.2/flux/Flux/Help/english/UserGuide/English/topics/BertottiIdentificationTool.htm>
- [30] C. Tan and L. Jing, "A Novel High Performance Magnetic Gear with Auxiliary Silicon Steel Sheet," *CES Transactions on Electrical Machines and Systems*, vol. 6, no. 2, pp. 201–206, 2022, doi: 10.30941/CESTEMS.2022.00027.

BIOGRAPHIES OF AUTHORS






d'Almeida Renaud Philippe    is an industrial Process Control Engineer. He received his research master's degree in electrical engineering from the Doctoral School of Engineering sciences at Abomey-Calavi University in 2020. He is currently pursuing a Ph.D. in electrical engineering. His research interests include the optimal design and control of electric machines, magnetic gears, and magnetically geared machines. He can be contacted at email: renaudjdd@yahoo.fr or renaudjdd@gmail.com.



Agbokpanzo Richard Gilles    CAMES University lecturer, is a Professor of Electrical Engineering at National University of Sciences, technology, Engineer and Mathematics. He is currently the head of Science and Industrial Technics department of Higher Normal School of Technical Education. His main research directions include electrical drives and optimization of electrical systems. He can be contacted at email: richgille@gmail.com or gilles.agbokpanzo@unstim.bj.



Agbomahena Bienvenu Macaire    is Professor in Applied Physics and Renewable Energy in Polytechnic School of University of Abomey-Calavi. He earned his master of physic sciences, Diploma of Advanced Studies DEA Electrotechnics, Ph.D. Sciences for Engineering option Energy and Environment at University of Abomey-Calavi (BENIN). Ph.D. of Sciences for University of Mons Umons in Belgium in 2013. His lectures include Energy and Environment, Renewable Energy-Organic Electronics-Electromagnetism-Materials for Energy Engineering. His primary research interests are in the field of organic photovoltaic device. He is currently Head of Electrical Engineering Department of Polytechnic School of University of Abomey-Calavi, Permanent Secretary of Scientific Committee on Engineering Science and Technology for University of Abomey-Calavi; WASEND Symposium and Seminar coordinator for CoEIE. He can be contacted at email: agbomac@yahoo.fr.